

Hybrid Analytical-FEM Approach for Power Transformer Transient Analysis

Bruno Jurišić, Zvonimir Jurković, Tomislav Župan, Mladen Marković

Summary — The paper describes a high-frequency model for transient calculation in transformer windings with segmentation on a turn level. The windings are represented by lumped RLC parameters given by the analytical approach, whereas the model is solved in the time domain. The accuracy of the analytical calculation is improved with correction factors obtained with a set of numerical calculations. The presented model is verified by measurements on the example of power transformer disc winding.

Keywords — transformer, transients, high-frequency model, inductance, capacitance.

I. INTRODUCTION

One of the key factors influencing the reliability and lifespan of power transformers is the quality and proper dimensioning of their insulation. In addition to nominal voltages, power transformers are susceptible to overvoltages resulting from lightning strikes or switching operations. During such events, the dielectric stress in insulation can be significantly increased. A properly designed insulation must withstand the impulse voltages according to international standards [1]. To dimension insulation properly during the insulation design phase, overvoltages and voltages inside transformer have to be calculated using suitable models.

Internal transient overvoltages within power transformers are typically calculated using white-box high-frequency models [2]. In these models, the windings are represented by lumped RLC parameters, which are calculated using analytical or numerical methods [3]. After modeling the winding using RLC parameters, i.e. electrical circuit, the resulting system of Kirchhoff equations is solved, either in the time or frequency domain. In the high-frequency model, the windings are segmented into elements, which can range from the entire winding down to the level of individual discs or turns. In the proposed model, windings are modeled at the turn level, which increases the accuracy of the model and enables direct calculation of detailed distribution of voltage within the winding. According to the reference [4], the valid frequency range of the high-frequency model is related to the length of the segments. The length of the segment should be at least four times smaller than the wavelength that corresponds to the highest frequency. The radius of the power transformer winding is typically up to one meter. There-

fore, the valid frequency range of the proposed model is approximately 10 MHz.

The calculation of RLC parameters is presented in Section II. The segmentation of the windings on a turn level implies the calculation of inductances (self and mutual), resistances and capacitances for each winding turn. There can be over thousands of turns in transformer windings, so methods that enable fast calculation are used. Capacitances are calculated using the analytical formulas and correction factors based on numerous 2D FEM calculations [5]. The inductances are calculated using the semi-analytical approach, based on work presented in papers [6-7]. The expressions given in these papers do not include infinite series [8], complex mathematical functions such as Bessel, Struve, and Legendre functions [9-10], or elliptic integrals [11]. Numerical integration, required in papers [6-7], is avoided by introducing the approximation of integral. The resistances, representing losses caused by skin and proximity effect, are calculated using the simple analytical formulas that can be found in the literature [12-13]. The model for magnetic field calculation, required for proximity loss calculation, is derived from Biot-Savart law. To validate the proposed model, a comparison is made against measurements conducted on the power transformer winding model, with details of the measurement setup shown in Section III and results presented in Section IV.

II. TRANSFORMER MODEL

The calculation of RLC parameters is presented in this section. The inductances and resistances are calculated using an air-core model that ignores the permeable core. This assumption is valid for calculation of high frequency overvoltages [4]. The capacitances are calculated using simple analytical formulas for plate capacitors and correction factors based on numerous 2D FEM calculations. After modeling the winding using the lumped RLC parameters, the nodal analysis in time domain is performed using the well-established Dommel's method [14].

A. CAPACITANCE

The capacitances between winding turns are calculated using the approach presented in reference [5]. The turn-to-turn capacitances are calculated between adjacent turns with significant capacitive coupling using simple analytical formulas for plate and cylindrical capacitors. Above-mentioned analytical formulas assume simplified geometry and homogeneous electric field which lead to inaccurate results. Therefore, correction factors, based on numerous 2D FEM calculations, are introduced to improve accuracy.

Permittivities of oil, paper and spacers are considered using the equivalent permittivity. It is important to emphasize that influence

(Corresponding author: Zvonimir Jurković)

Bruno Jurišić, Zvonimir Jurković and Tomislav Župan are with the Končar - Electrical Engineering Institute Ltd., Zagreb, Croatia (e-mails: bjurisic@koncar-institut.hr, zjurkovic@koncar-institut.hr, tzupan@koncar-institut.hr)

Mladen Marković is with the Končar – Distribution and Special Transformers Inc., Zagreb, Croatia (e-mail: Mladen.Markovic@koncar-dst.hr)

of additional materials inside transformer winding, such as spacers, on overvoltage waveforms is not negligible.

B. INDUCTANCE

The mutual inductance of two coaxial coils with rectangular cross-sections can be calculated as a linked flux in one coil, whereas there is a current of one ampere in the other coil (source of magnetic flux). The linked flux can be calculated from vector magnetic potential using the expression:

$$\phi = \oint \mathbf{A} d\mathbf{l}, \quad (1)$$

whereas the vector magnetic potential is related to the source current by integral of Green's function for vector magnetic potential:

$$\mathbf{A}(\mathbf{r}) = \frac{\mu_0}{4\pi} \int \frac{\mathbf{J}(\mathbf{r}')}{|\mathbf{r} - \mathbf{r}'|} d^3 \mathbf{r}' \quad (2)$$

The expression (2) can be applied to the axisymmetric geometry shown in Fig. 1. The current density $\mathbf{J} = \frac{1A}{S_1} (S_1 = (r_2 - r_1)(z_2 - z_1))$

is cross-section of first coil) inside first coil is integrated with respect to variables $r, z,$ and φ to get the vector magnetic potential inside the region of the second coil. The vector magnetic potential inside the second coil is integrated with respect to variables R and Z (due to axisymmetric geometry, integration with respect to φ comes down to multiplication by 2π) and divided by cross-section of other coil $S_2 = (r_4 - r_3)(z_4 - z_3)$ to get the flux linkage of second coil, i.e. the mutual inductance between first and second coil. By combining the expressions (1) and (2), and the definition that the mutual inductance is equal to flux linked in one coil, whereas the current of one ampere is in the other coil, the following expression is obtained:

$$L_{12} = \frac{\mu_0}{S_1 S_2} \int Q(r, R, z, Z, \varphi) dr dR dz dZ d\varphi \quad (3)$$

where function $Q(r, R, z, Z, \varphi)$, for considered geometry, is given as

$$Q(r, R, z, Z, \varphi) = \frac{rR \cos(\varphi)}{\sqrt{r^2 + R^2 - 2rR \cos(\varphi) + (z - Z)^2}} \quad (4)$$

In references [6-7], integral (3) is solved analytically with respect to variables $r, R, z,$ and Z . That function's arguments are coils' geometry parameters $r_1, r_2, r_3, r_4, z_1, z_2, z_3, z_4,$ and azimuthal variable φ . That function is denoted by G , whereas the arguments, except for the azimuthal variable φ , are left out for the sake of conciseness.

The goal is to obtain the approximation of integral:

$$L_{12} = \frac{\mu_0}{S_1 S_2} \int_{\varphi=0}^{\pi} G(\varphi) d\varphi \quad (5)$$

in closed-form to enable calculation of L matrix on turn level in acceptable time range. Function $G(\varphi)$ is equal to integral of $Q(r, R, z, Z, \varphi)$ with respect to variables $r, R, z,$ and Z . Detailed derivation of function $G(\varphi)$ is given in [6-7].

A G function has a characteristic shape with the following properties:

- The function has a maximum at point $\varphi=0$ (from now on denoted as G_0) and minimum at point $\varphi=\pi$ (from now on denoted as G_π).
- The function is monotonically decreasing.
- Value of G function at point $\varphi = \frac{\pi}{2}$ is equal to zero.
- Absolute value of G_π is smaller than G_0 .

Examples of G function, for different geometries of coils, are shown in Fig. 2. Physically, G function with narrow shape of positive part of the function and small ratio $\frac{G_\pi}{G_0}$ corresponds to the coils that are close to each other. By increasing the distance between coils, the shape of G function is closer to the cosine. The approximation of the integral of the G function assumes that the integral value can be correlated with the ratio $\frac{G_\pi}{G_0}$.

To get the approximation of integral (5), numerous calculations of G function's integral, using expressions from paper [7], were performed. Then, integral value is expressed using the rational functions, where the coefficients of the numerator and denominator polynomials were obtained using the least squares method:

$$\int_{\varphi=0}^{\pi} G(\varphi) d\varphi \approx G_0 \left[\frac{0.008618 \left(\frac{G_\pi}{G_0}\right)^3 + 9.711 \left(\frac{G_\pi}{G_0}\right)^2 + 159.6 \frac{G_\pi}{G_0} + 75.62}{\left(\frac{G_\pi}{G_0}\right)^3 + 35.03 \left(\frac{G_\pi}{G_0}\right)^2 + 131.3 \frac{G_\pi}{G_0} + 77.74} - \frac{1.07 \frac{G_\pi}{G_0} - 0.5949}{\left(\frac{G_\pi}{G_0}\right)^2 - 0.5201 \frac{G_\pi}{G_0} - 0.002404} \right] \quad (6)$$

Above-mentioned expressions can be used to calculate the self-inductance. In that case, geometrical parameters are $r_1 = r_1 + \Delta, r_2 = r_2 + \Delta, z_3 = z_1 + \Delta,$ and $z_4 = z_2 + \Delta$. Small displacement Δ is added to avoid singularities, which are explained in papers [6-7]. In this paper, that displacement is $\Delta = 10^{-6}$.

Expressions for G_0 and G_π are given in papers [6-7].

C. RESISTANCE

The resistances in the proposed model include DC resistance, and AC resistances that represent losses due to skin and proximity effects. The resistance per unit length that takes skin effect into account is calculated using the expression [13]

$$R'_{skin} = \frac{1}{4\sigma(h+w)^2} \left[\frac{h \sinh\left(\frac{2w}{\delta}\right) + \sin\left(\frac{2w}{\delta}\right)}{\delta \cosh\left(\frac{2w}{\delta}\right) + \cos\left(\frac{2w}{\delta}\right)} + \frac{w \sinh\left(\frac{2h}{\delta}\right) + \sin\left(\frac{2h}{\delta}\right)}{\delta \cosh\left(\frac{2h}{\delta}\right) + \cos\left(\frac{2h}{\delta}\right)} + 2 \right] \quad (7)$$

where w and h are width and height of the conductor, respectively. If the conductor consists of more separately insulated wires (e.g. continuously transposed conductor), resistance for each wire is calculated separately. The parameter σ is the electrical conductivity of conductor, and the parameter $\delta = \sqrt{\frac{1}{\pi f \mu_0 \sigma}}$ is the skin depth of conductor. R matrix is calculated at arbitrarily chosen frequency $f=10$ kHz.

To calculate the losses due to proximity effect, magnetic field at the position of another coil (r_0, z_0) must be calculated. The geometry of windings is simplified to get simple mathematical expressions. The permeable core is neglected and the geometry of winding is assumed to be planar (see Fig. 3). Expressions for magnetic field are derived from Biot-Savart law:

$$\mathbf{B}(\mathbf{r}) = \frac{\mu_0}{4\pi} \int \frac{I d\mathbf{l} \times \mathbf{r}'}{|\mathbf{r}'|^3} \quad (8)$$

For the geometry shown in Fig 3 (infinitely long coil of rectangular cross-section with current of one ampere), Biot-Savart (8) can be written as:

$$B(r_0, z_0) = \frac{\mu_0}{4\pi(r_2 - r_1)(z_2 - z_1)} \int_{l=-\infty}^{\infty} \int_{z_1}^{z_2} \int_{r_1}^{r_2} \frac{(z_0 - z) \bar{a}_r - (r_0 - r) \bar{a}_z}{\sqrt{l^2 + (r_0 - r)^2 + (z_0 - z)^2}} dl dr dz. \quad (9)$$

By solving the integral (9), and components of the magnetic field are obtained:

$$B_r = k \left[\left((r_0 - r) \ln((r_0 - r)^2 + (z_0 - z)^2) + 2(z_0 - z) \tan^{-1} \left(\frac{r_0 - r}{z_0 - z} \right) \right) + \left((r_0 + r) \ln((r_0 + r)^2 + (z_0 - z)^2) + 2(z_0 - z) \tan^{-1} \left(\frac{r_0 + r}{z_0 - z} \right) \right) \right] \Big|_{r=r_1}^{r_2} \Big|_{z=z_1}^{z_2}, \quad (10)$$

$$B_z = k \left[\left((z_0 - z) \ln((z_0 - z)^2 + (r_0 - r)^2) + 2(r_0 - r) \tan^{-1} \left(\frac{z_0 - z}{r_0 - r} \right) \right) + \left((z_0 - z) \ln((z_0 - z)^2 + (r_0 + r)^2) + 2(r_0 + r) \tan^{-1} \left(\frac{z_0 - z}{r_0 + r} \right) \right) + 4z \right] \Big|_{r=r_1}^{r_2} \Big|_{z=z_1}^{z_2}, \quad (11)$$

$$k = \frac{\mu_0}{4\pi(r_2 - r_1)(z_2 - z_1)}. \quad (12)$$

After the calculation of magnetic field, the losses (equal to resistance since current in first coil is one ampere) due to proximity effect per unit length are calculated separately for each component of the magnetic field. For that purpose, simple, well-known expressions for eddy-current losses (per unit volume) in infinite planar plate of thickness t and conductivity σ (page 154 in [12]) are used:

$$p = \frac{(2\pi f)^2 B^2 t^2 \sigma}{24} \quad (13)$$

By combining the expressions (10-14), the resistance per unit length is calculated as:

$$R'_{proximity} = \frac{\sigma \pi^2 f^2 (B_r^2 h^3 w + B_z^2 w^3 h)}{6} \quad (14)$$

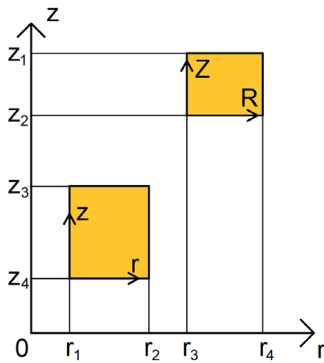


Fig. 1. The geometry of two circular coaxial coils with rectangular cross-sections

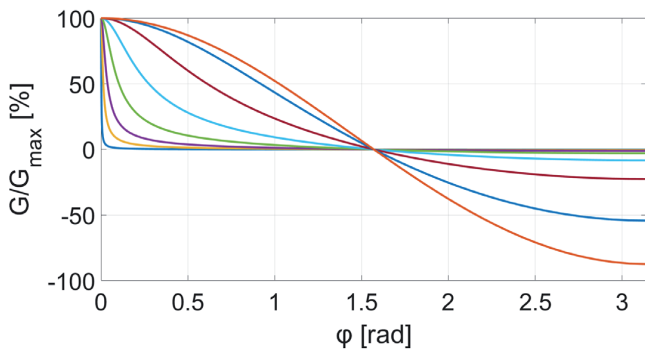


Fig. 2. The examples of G function for different coil's geometries

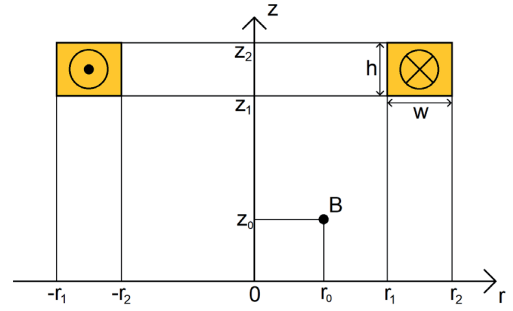


Fig. 3. The geometry of model for calculation of magnetic field

III. MEASUREMENTS ON POWER TRANSFORMER WINDING MODEL

To verify the proposed methodology, the overvoltages are measured on the power transformer winding model (see Fig. 4). The model includes two axially stacked disc windings that are pressed between two steel plates, with no tank or oil. The upper winding has 48 discs and 9 conductors in disc, whereas the bottom winding has 48 discs and 10 conductors in disc. The standard impulse test wave 1.2/50 μ s is generated using the surge generator *Haefely type 48t*. To enable measurement of voltage along the winding, insulation is removed and copper terminals are soldered in 48 places. Then, voltage waveforms at these terminals are measured using the oscilloscope *Tektronix DPO 4054* and measuring probes. The measurement setup is illustrated in Fig. 5.



Fig. 4. The winding model

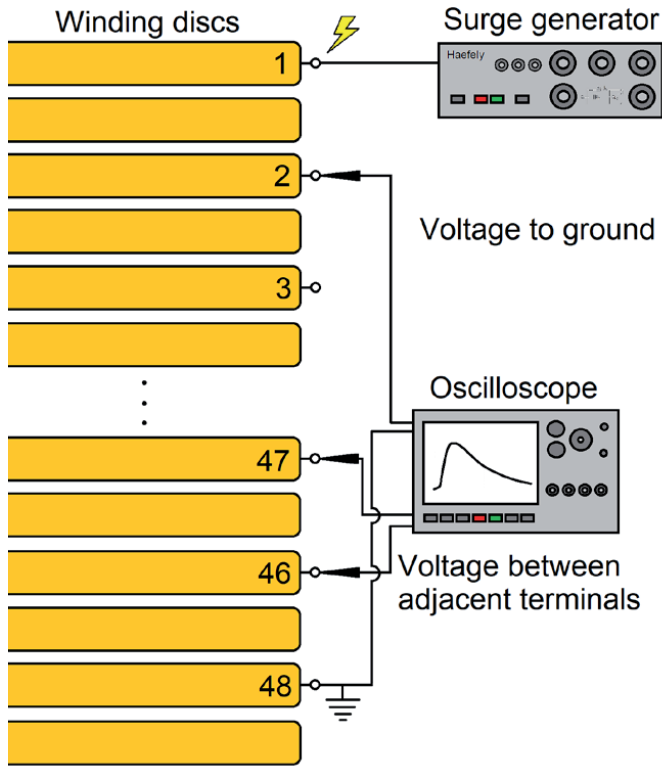


Fig. 5. The measurement setup

IV. MATHEMATICAL MODEL RESULTS

The overvoltages along the winding model are calculated using the methodology proposed in Section II. The results are compared against the measurements. Then, the visualization of voltages in the winding, using color mapping, is presented.

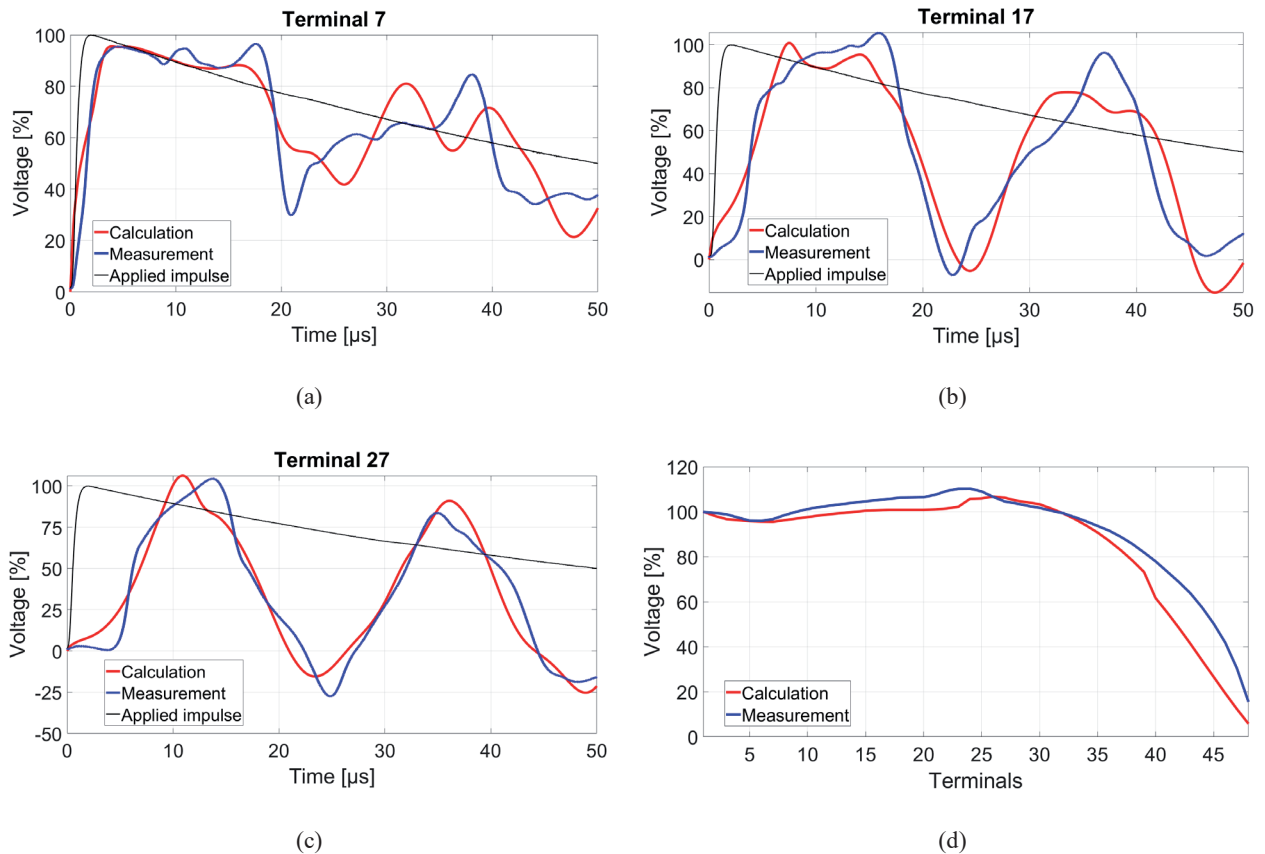


Fig. 6. The voltage waveforms at terminals 7 (a), 17 (b), 27 (c), and distribution of maximum voltages to ground along the winding (d)

A. MODEL VERIFICATION

The calculated voltage waveforms at three terminals and distribution of maximum voltages to ground along the winding are compared against the measurements. The comparison is shown in Fig. 6.

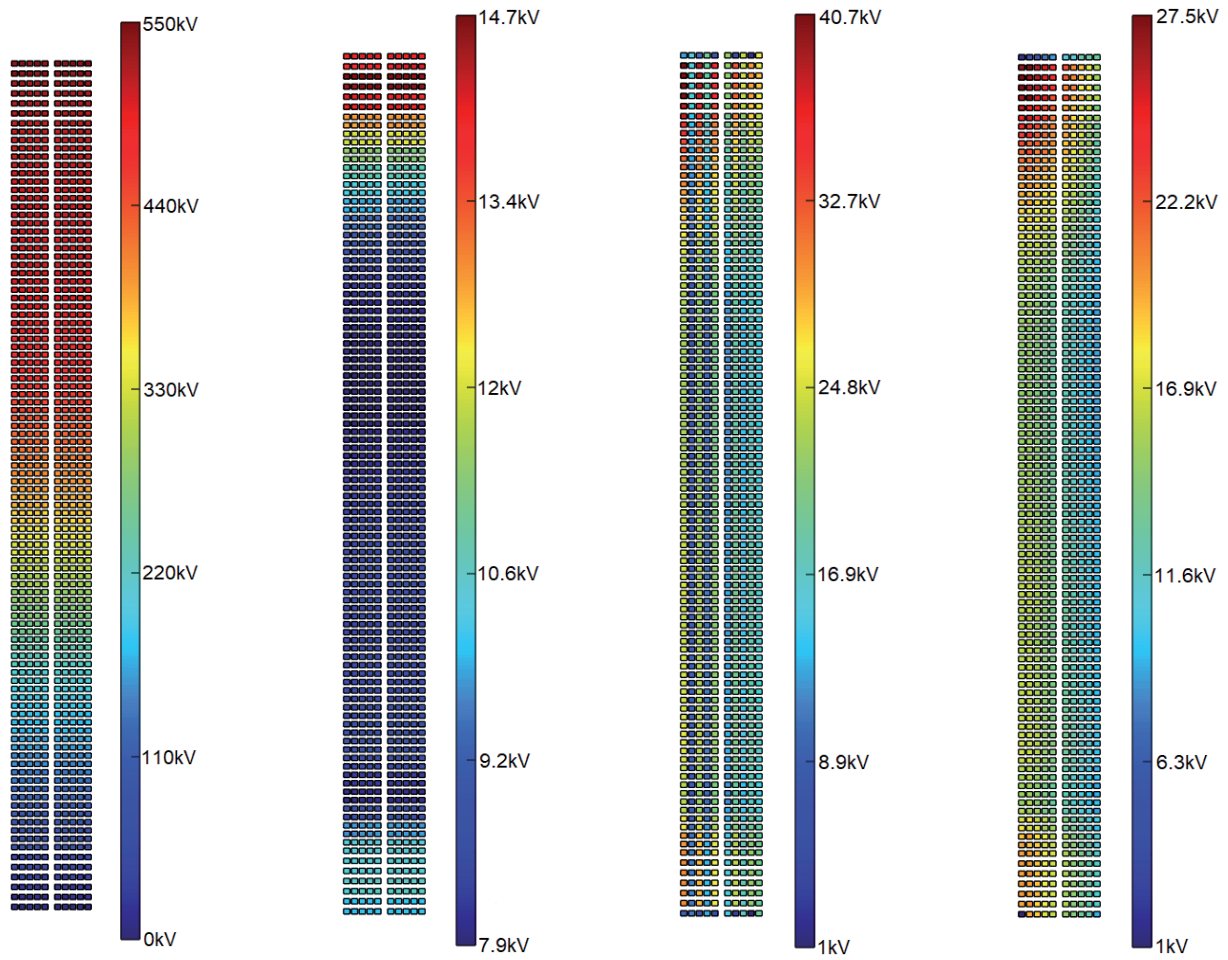
The error for maximum values of voltages, shown in Fig. 6, are given in Table I.

TABLE I.
RELATIVE ERRORS FOR MAXIMUM VALUES OF VOLTAGES

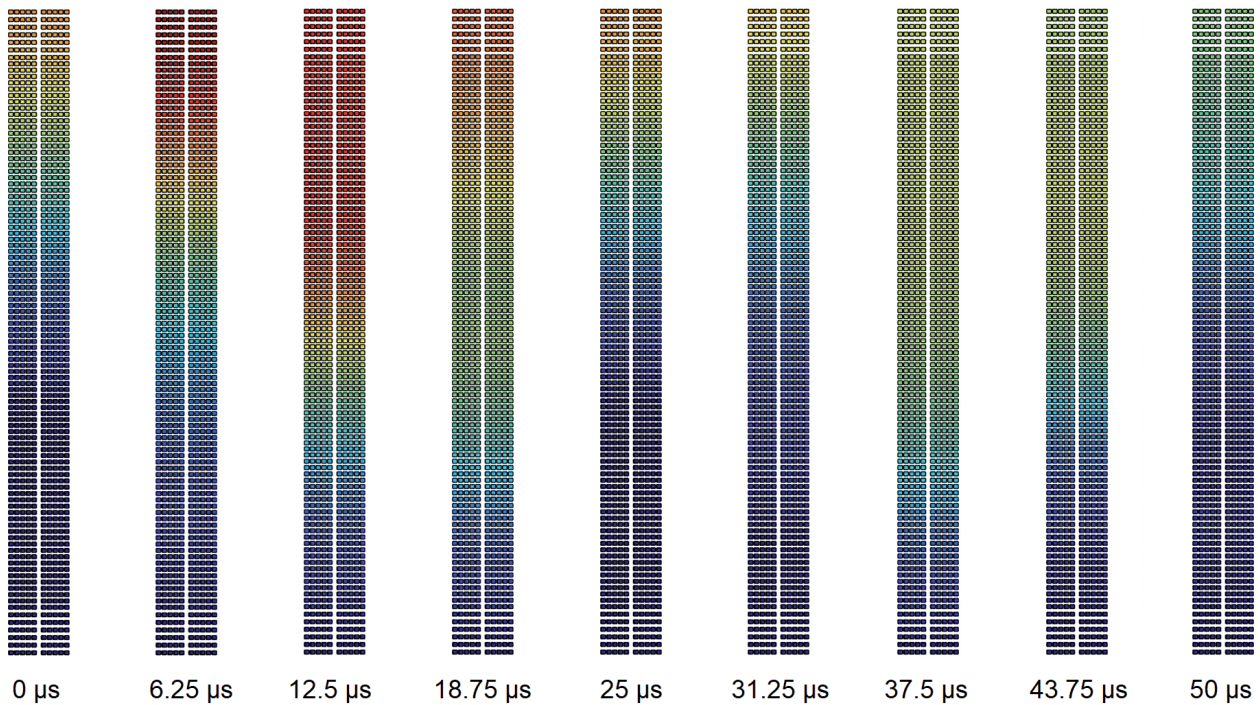
	Error [%]
Terminal 7 waveform	-1.2
Terminal 17 waveform	-4.6
Terminal 27 waveform	1.7
Distribution along winding	-3.2

B. VISUALIZATION OF VOLTAGES IN THE WINDING

The proposed model enables the calculation of voltage waveforms for every single turn. Such detailed results can be represented in various ways, numerically and visually. Spatial distribution of voltage can be represented visually for the entire winding using color mapping. Maximum voltages to ground and voltages between adjacent turns (radially, axially and diagonally) of interleaved winding with radial and axial channel are shown in Fig. 7. Except maximum values, voltage values can be shown for every time step. By taking series of images with voltage values for every time step, animation can be generated that shows behavior of voltage in space and time (for example, propagation and reflections of transient wave can be shown).



(a) (b) (c) (d)



(e)

Fig. 7. The representation of maximum voltages to ground (a), and between radially (b), axially (c) and diagonally (d) adjacent turns. Propagation of transient wave is shown by series of images with instantaneous values of voltage (e)

V. CONCLUSION

The methodology for calculation of transient overvoltages in a power transformer is presented in the paper. The transformer winding is modeled down to the level of turn, using lumped RLC parameters. The model is solved in time domain using Dommel's method. The capacitances are calculated using simple analytical models and correction factors based on the 2D FEM. The inductances and resistances are calculated using analytical models that neglect the permeable core, which is valid when calculating high frequency transients. The proposed methodology enables fast calculations even with complicated transformer winding geometries with thousands of turns. The calculation of RLC parameters is in a time range of seconds, whereas the calculation in the time domain is in a time range of tens of seconds. That makes the proposed methodology suitable for application in the transformer design process.

The mathematical expressions for the calculation of inductances are derived using the Green's function for vector magnetic potential. To derive the expressions, multiple integral with respect to five variables must be solved. In the existing literature, integral is solved with respect to four variables, whereas numerical integration with respect to the fifth variable is necessary. To avoid numerical integration, approximation of the unsolved integral is introduced. The resistances are calculated using simple analytical expressions from the existing literature. However, the model for calculation of the magnetic field is derived from the Biot-Savart law with assumption of planar geometry of windings. The closed-form expressions for inductances and resistances, with no need for numerical integration, allow very fast calculations.

The measurements of overvoltage distribution on the experimental winding model are done to verify the proposed approach. The comparison between calculation and measurement results has shown good accuracy of the proposed model, as in the worst case the amplitude error is less than five percent. The possibility of detailed visualization of voltage in the winding is presented. Except standard representation of results, such as numerical data or 2D plots of waveforms, detailed visualization of voltages in the windings or between the windings can be a very helpful tool for power transformer design engineers.

REFERENCES

- [1] "IEC 60060-1", High-voltage test techniques Part 1: General definitions and test requirements, 2010
- [2] E. E. Mombello, G. A. Díaz Flórez, "An improved high frequency white-box lossy transformer model for the calculation of power systems electromagnetic transients," in *Electric Power Systems Research*, vol. 190, Jan. 2021, doi: 10.1016/j.epsr.2020.106838.
- [3] T. Župan, B. Trkulja, R. Obrist, T. Franz, B. Cranganu-Cretu and J. Smajic, »Transformer Windings' RLC Parameters Calculation and Lightning Impulse Voltage Distribution Simulation,« in *IEEE Transactions on Magnetics*, vol. 52, no. 3, pp. 1-4, March 2016, Art no. 8400204, doi: 10.1109/TMAG.2015.2481004.
- [4] CIGRE JWG A2/C4.52., "High Frequency Transformer and Reactor Models for Network Studies – Part A: White-Box Models", CIGRE, technical brochure, 2023.
- [5] Z. Jurković, B. Jurišić, M. Marković and T. Župan, »Improved Analytical Calculation of Winding Capacitance Using Correction Factors,« *2022 7th International Advanced Research Workshop on Transformers (ARWtr)*, Baióna, Spain, 2022, pp. 30-35, doi: 10.23919/ARWtr54586.2022.9959895.
- [6] T. Župan, Ž. Štih and B. Trkulja, »Fast and Precise Method for Inductance Calculation of Coaxial Circular Coils With Rectangular Cross Section Using the One-Dimensional Integration of Elementary Functions Applicable to Superconducting Magnets,« in *IEEE Transactions on Applied Superconductivity*, vol. 24, no. 2, pp. 81-89, April 2014, Art no. 4901309, doi: 10.1109/TASC.2014.2301765.
- [7] S. Liang and Y. Fang, »Analysis of Inductance Calculation of Coaxial Circular Coils With Rectangular Cross Section Using Inverse Hyperbolic Functions,« in *IEEE Transactions on Applied Superconductivity*, vol. 25, no. 4, pp. 1-9, Aug. 2015, Art no. 4901209, doi: 10.1109/TASC.2015.2427353.
- [8] Dwight, H., Chen, S., "An extension of a maxwell mutual-inductance formula to apply to thick solenoids", *Journal of Applied Physics*, Vol. 4, No. 9, 1933, str. 323–326.
- [9] Conway, J. T., "Inductance calculations for circular coils of rectangular cross section and parallel axes using Bessel and Struve functions", *Magnetics, IEEE Transactions on*, Vol. 46, No. 1, 2010, str. 75–81.
- [10] Hurley, W. G., Duffy, M. C., "Calculation of self and mutual impedances in planar magnetic structures", *Magnetics, IEEE Transactions on*, Vol. 31, No. 4, 1995, str. 2416–2422.
- [11] Garrett, M. W., "Calculation of fields, forces, and mutual inductances of current systems by elliptic integrals", *Journal of Applied Physics*, Vol. 34, No. 9, 1963, str. 2567–2573.
- [12] S. V. Kulkarni, »Transformer Engineering: Design, Technology and Diagnostics«, CRC Press., Second Edition, 2012.
- [13] R. L. Stoll, *The Analysis of Eddy Currents*. Oxford: Oxford University Press, 1974.
- [14] H. W. Dommel, »Digital Computer Solution of Electromagnetic Transients in Single-and Multiphase Networks,« in *IEEE Transactions on Power Apparatus and Systems*, vol. PAS-88, no. 4, pp. 388-399, April 1969, doi: 10.1109/TPAS.1969.292459.